applied sciences

MDPI

Article

Design of an Optimized Terahertz Time-Domain Spectroscopy System Pumped by a 30 W Yb:KGW Source at a 100 kHz Repetition Rate with 245 fs Pulse Duration

Lennart Hirsch [1,*], Dionysis Adamou [1], Daniele Faccio [2], Marco Peccianti [3] and Matteo Clerici [1,4,*]

[1] James-Watt School of Engineering, Advanced Research Centre, University of Glasgow, Glasgow G11 6EW, UK
[2] School of Physics and Astronomy, Advanced Research Centre, University of Glasgow, Glasgow G11 6EW, UK
[3] Emergent Photonics Research Centre, Department of Physics, Loughborough University, Loughborough LE11 3TU, UK
[4] Dipartimento di Scienza e Alta Tecnologia, Università degli Studi dell'Insubria, 22100 Como, Italy
* Correspondence: l.hirsch.1@research.gla.ac.uk (L.H.); matteo.clerici@uninsubria.it (M.C.)

Abstract: Ytterbium laser sources are state-of-the-art systems that are increasingly replacing Ti:Sapphire lasers in most applications requiring high repetition rate pulse trains. However, extending these laser sources to THz Time-Domain Spectroscopy (THz-TDS) poses several challenges not encountered in conventional, lower-power systems. These challenges include pump rejection, thermal lensing in nonlinear media, and pulse durations exceeding 100 fs, which consequently limit the detection bandwidth in TDS applications. In this article, we describe our design of a THz-TDS beamline that seeks to address these issues. We report on the effectiveness of temperature controlling the Gallium Phosphide (GaP) used to generate the THz radiation and its impact on increasing the generation efficiency and aiding pump rejection while avoiding thermal distortions of the residual pump laser beam. We detail our approach to pump rejection, which can be implemented with off-the-shelf products and minimal customization. Finally, we describe our solution based on a commercial optical parametric amplifier to obtain a temporally compressed probe pulse of 55 fs duration. Our study will prove useful to the increasing number of laboratories seeking to move from the high-energy, low-power THz time-domain spectroscopy systems based on Ti:Sapphire lasers, to medium-energy, high-power systems driven by Yb-doped lasers.

Keywords: terahertz; spectroscopy; Gallium Phosphide; femtosecond; ytterbium lasers

Citation: Hirsch, L.; Adamou, D.; Faccio, D.; Peccianti, M.; Clerici, M. Design of an Optimized Terahertz Time-Domain Spectroscopy System Pumped by a 30 W Yb:KGW Source at a 100 kHz Repetition Rate with 245 fs Pulse Duration. *Appl. Sci.* **2024**, *14*, 6688. https://doi.org/10.3390/app14156688

Academic Editor: Matt Oehlschlaeger

Received: 11 July 2024
Revised: 25 July 2024
Accepted: 29 July 2024
Published: 31 July 2024

1. Introduction

Terahertz Time-Domain Spectroscopy (THz-TDS) is a spectroscopic technique that yields a direct measurement of the electric field of the probing THz radiation. The resulting trace contains both the amplitude and phase information of its frequency components, instead of only the power at each frequency, as is the case in conventional frequency-domain spectroscopy techniques. This allows for the determination of optical constants without the application of Kramers–Kronig relations [1,2]. THz-TDS has strong applications in many fields [3], including biological and chemical sensing [4], the detection and classification of drugs and explosives [5,6], the characterisation of semiconductors [7], food quality testing [8] and many more.

Broadband THz radiation may be generated through several techniques, the most common being generation by photoconductive antenna (PCA), by semiconductor superlattice multipliers [9,10], by optical rectification (OR), and by plasma [1,11]. As PCAs are designed for use with optical powers on the order of mW (with the exception of some antenna designs such as large area PCAs [12,13], which push optical powers close to the Watt-level), THz generation by optical rectification and via two-colour plasma generation

are generally used with higher average pumping power. Air plasma allows for the generation of extremely broad THz bandwidths with high, MV/cm peak electric fields at a kHz repetition rate [14]. However, pulse energies greater than 100 µJ and durations shorter than 100 fs are required for effective broadband generation [15]. In addition, the generation of THz by gas ionization with a high repetition rate and high average power sources faces issues associated with the gas dynamics driven by the pump laser [16]. As such, optical rectification is more commonly used when generating THz using high average power pumps. In these systems, a single cycle THz pulse is generated by the optical pulse in a nonlinear crystal— often a zinc blend crystal such as Gallium Phosphide (GaP). To efficiently generate THz pulses by optical rectification, matching between the group velocity of the optical pump and the phase velocity of the THz wave must be achieved. This requirement imposes the use of tilted optical pulses when highly efficient Lithium Niobate crystals are employed, either excited by Ti:Sapphire lasers at ∼800 nm [17] or, more recently, by Yb-doped lasers at ∼1 µm [18,19]. On the other hand, if lower generation efficiencies can be tolerated, optical rectification is naturally group-phase-matched when pumping GaP crystals at around 1 µm [20,21]. Despite the lower efficiency ($\simeq 10^{-5}$) and higher absorption from free carriers, with its first phonon absorption peak at 11 THz (compared to 5.32 THz for ZnTe) [22], GaP is a popular medium for THz generation as it allows for broadband generation with relatively simple THz source geometries.

2. Conventional Approach to THz-TDS

The conventional THz beamline, shown schematically in Figure 1, consists of the THz source, a beam-routing section composed of 90° off-axis parabolic mirrors, and the detection stage. The THz radiation is generated via rectification in an electro-optic medium such as GaP. In this experiment, a 1 mm thick antireflection-coated GaP crystal cut in the 110 plane was used for generation (UniversityWafer, Boston, MA, USA). The pump is injected into the GaP crystal and, after THz generation, is removed using filters [15,23] or via a hole in the first parabolic mirror [22,24]. This hole is commonly 3 mm in diameter as mirrors with these specifications are readily available from manufacturers; smaller diameter holes generally require custom fabrication. Due to the non-spherical geometry of these mirrors, it is difficult to manufacture parabolic mirrors with custom specifications unless carried out in large batch sizes. Stray pump light may be rejected using filters such as high-resistivity float zone silicon (FZSi) [25] placed at Brewster's angle, PTFE, or even paper. These materials are transparent to THz but reflect or absorb the pump light. However, the use of Silicon filters is not ideal in the case of high-power Yb-doped lasers due to the proximity of the silicon bandgap with the laser's photon energy (1.203 eV at 1030 nm vs. 1.124 eV at 300 K) [26].

A second parabolic mirror refocuses the collimated THz radiation into a sampling spot; this is where a sample may be placed for spectroscopic measurements. Finally, a third and fourth parabolic mirror recollimate and refocus the THz radiation into the detection plane. Here, the THz radiation is focused onto an electro-optic crystal and overlaps spatially with the probe beam. A GaP wafer cut in the 110 plane with a thickness of 300 µm (Pi-Kem, Tamworth, UK) was used in this case. The temporal overlap is controlled using a delay line stage. A standard polarimetry setup is employed to record the THz-induced polarisation rotation as a function of the delay between the THz pulse and the sampling (probe) ultrashort pulse—see [27] for a recent discussion, and a lock-in amplifier (synchronized to the amplitude modulation induced on the THz field via an optical chopper) is used to reduce background noise.

To avoid THz losses and signal contamination due to water absorption, purging with nitrogen gas is employed to remove humidity from the atmosphere. This results in an increased signal strength (a 2–3 times greater peak signal has been observed in our case) and the suppression of the ringing signal originating from resonances in atmospheric water.

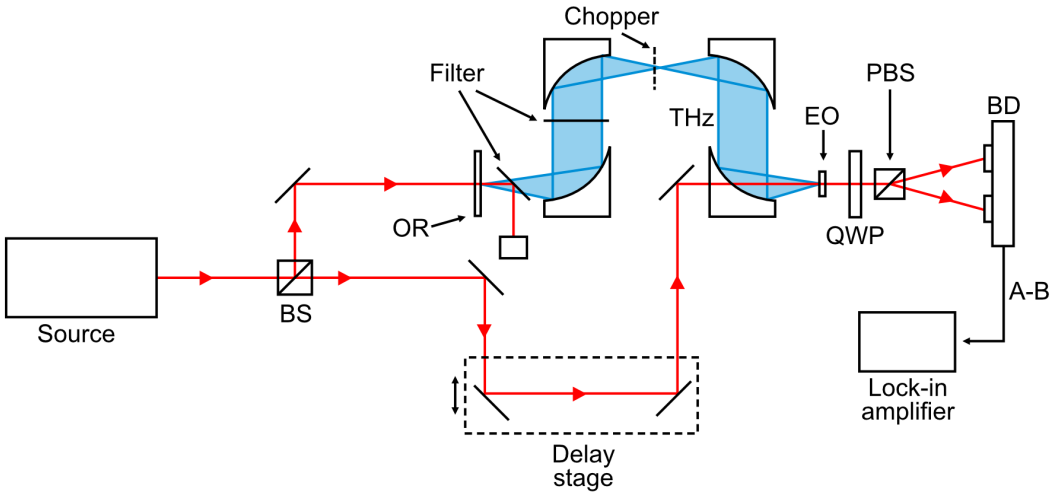

Figure 1. Conventional THz-TDS beamline. BS: Beamsplitter; OR: Optical rectification via GaP crystal; EO: electro-optic wafer; QWP: quarter-wave plate; PBS: polarising beam splitter (Wollaston prism); BD: balanced detector.

To maximize the THz-TDS signal, the optical-to-THz conversion efficiency must be maximized. To this end, the pulse intensity on the generating crystal should be such that the conversion is close to nonlinear saturation at the highest possible energy per pulse. This defines an ideal beam size. When using a high-power pump beam, the ideal beam size may be larger than the rejection hole in the first parabolic mirror; this was indeed the case in our system. This can result in the clipping of the pump beam on the pump rejection hole and hence in scattered pump light that, at high powers, has the potential of warping or burning filters used to remove the residual scattered radiation, or even affecting the tested sample. Off-axis parabolic mirrors with larger holes are difficult to obtain and are undesirable as they result in a larger loss of THz radiation through the hole. With a pump energy at 150 µJ, after optimizing the pump beam size for maximal THz generation efficiency (3.5 mm $1/e^2$), we measured with a thermal detector ≃22% of the residual pump in the beam path after reflection off a parabolic mirror with a 3 mm diameter hole. It is also to be noted that high pump powers result in thermal lensing in the generation crystal, leading to a degradation of the pump beam quality [28], which makes geometrical pump rejection more challenging, as shown in Section 5.

3. Optimization of the Conversion Efficiency

The optical conversion efficiency of THz generation via rectification in GaP is typically on the order of 10^{-7}–10^{-5} [29–33]. For maximal THz generation, the pulse intensity in the crystal should be optimized by targeting the saturation intensity, where nonlinear losses quench any further increase in the conversion efficiency at increasing pump intensities. In our experimental setting, this condition translates into finding the beam size for which the conversion efficiency saturates at the maximum available pump energy, i.e., 300 µJ, corresponding to 30 W at our fixed 100 kHz.

To this end, the rectification conversion efficiency was recorded at increasing pump powers and fixed beam size. This process was repeated for three different $1/e^2$ beam diameters: 0.88 mm, 1.05 mm, and 3.50 mm. The THz power was recorded with a pyroelectric detector (Gentec THZ5I-BL-BNC, Gentec-EO, Québec City, QC, Canada) while the pump power was measured with a thermal detector (Gentec UP25N-100H-H9-D0, Gentec-EO, Québec City, QC, Canada).

It was found that, for our GaP crystal, (1 mm thick, 110-cut, antireflection-coated GaAs, UniversityWafer) pumped by 1030 nm pulses with a duration of 245 fs at a repetition rate of 100 kHz (Light Conversion Carbide CB3-40W, Light Conversion, Vilnius, Lithuania), the conversion efficiency saturated at $\simeq 7 \times 10^{-7}$ for a 30 W pump power when using an

optimal beam diameter of around 3.5 mm $1/e^2$, as shown in Figure 2. We note that the conversion efficiency in our experiment is lower than what is reported in record-breaking experiments, e.g., [32], as our laser pulses are longer and the efficiency scales with the driving pulse duration τ as $1/\tau^2$ [34,35].

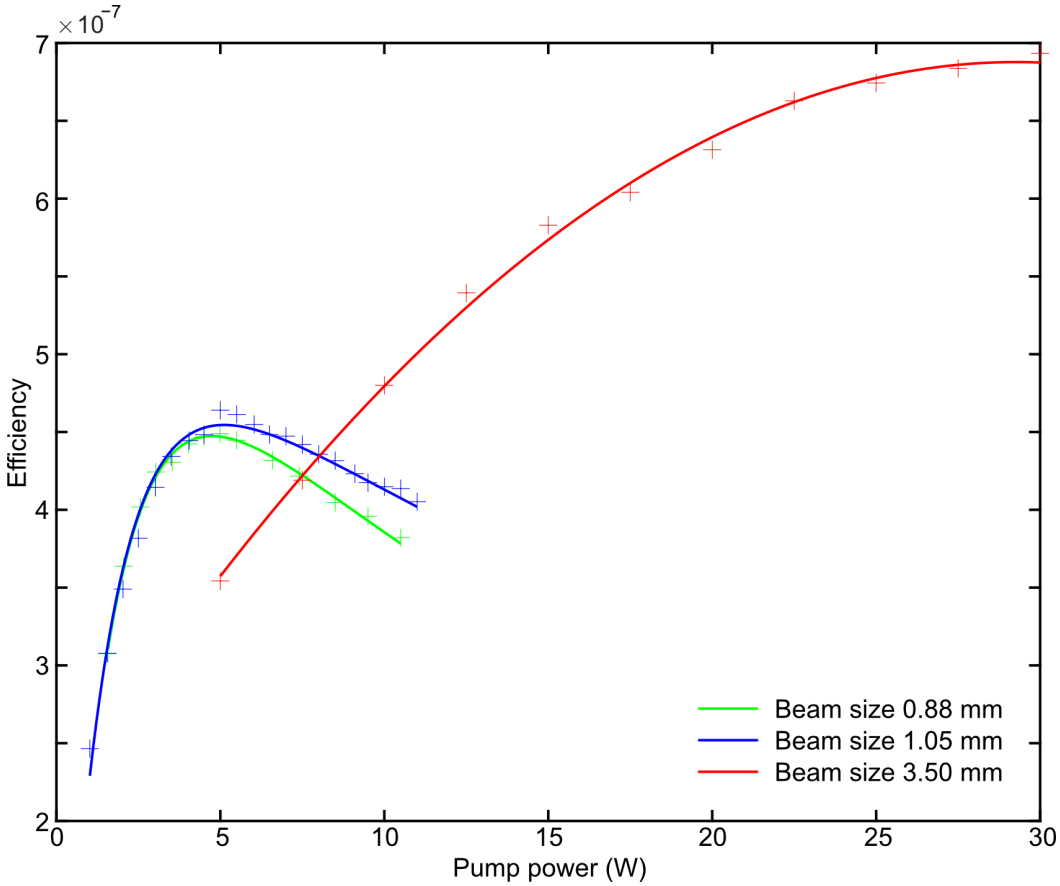

Figure 2. Generation efficiency for increasing pump power. The optimal condition in our experiment was reached with a 3.5 mm $1/e^2$ diameter pump beam (red curve), for which the conversion efficiency was saturated at 30 W, the maximum laser power available for pumping the rectification process. As a comparison, we show that the conversion efficiency saturates at lower powers for smaller beam sizes (blue and green data).

4. Beamline Design

One of the main technical challenges associated with a THz-TDS driven by a medium-energy, high-power pump laser is the rejection of the optical pump from the generated THz beam-path. While custom-designed parabolic mirrors associated with geometrical filtering and further filtering with paper foils, as carried out, e.g., [32], provide a potential solution to the problem, we sought to build our THz-TDS with off-the-shelf components—specifically 2-inch-diameter off-axis parabolic mirrors (Thorlabs, Newton, NJ, USA) and flat copper mirrors (LBP-Optics, Biggleswade, UK) and only minimal customization, with the two-fold objective of removing the optical pump while preserving as much as possible the generated THz power.

We designed the THz-TDS beamline to allow for geometrical pump rejection with limited THz losses. Given our pump beam's size and the results of knife-edge measurements of the generated THz beam, we concluded that a propagation distance of $\simeq$450 mm would be required to expand the THz beam to a diameter of 50.8 mm, filling the aperture of the parabolic mirrors. The best matching off-the-shelf product we could source was a 15° off-axis parabolic mirror with an equivalent focal length of 15″ (381 mm).

We numerically investigated the effect of such a choice on the focused THz beam quality, resulting in the design shown in Figure 3. The expected beam size for a 1.5 THz beam is 330 × 316 µm in the detection plane, with phase profile variations of a few tenths of a radian across the beam, confirmed by physical optics propagation simulations performed on the beamline design and shown in Figure 4.

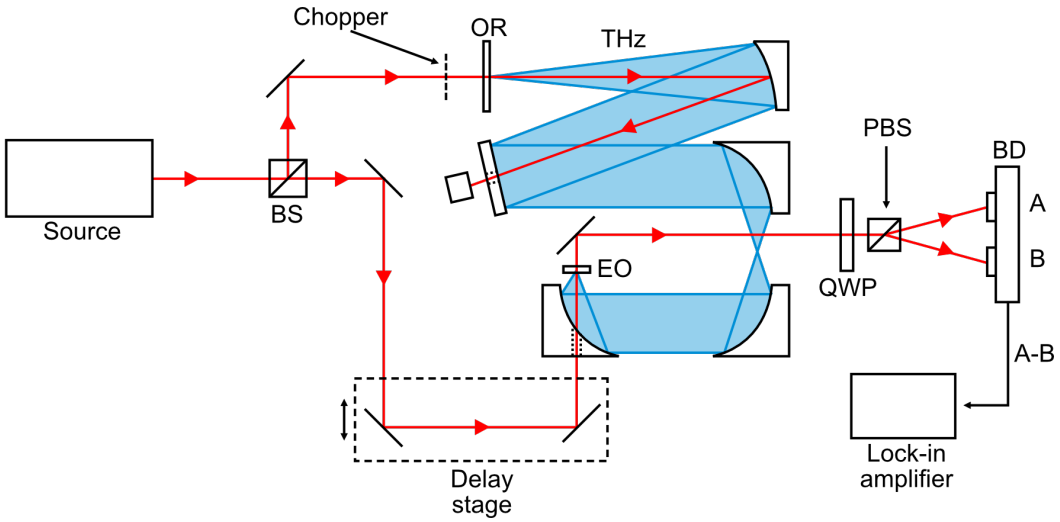

Figure 3. A schematic of our low-loss THz-TDS beamline utilizing a long focal length parabolic and a flat pump rejection mirror.

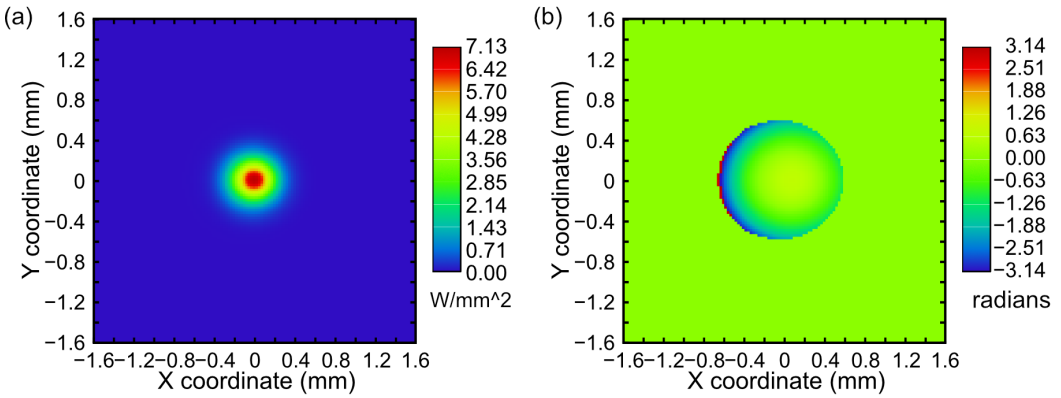

Figure 4. Simulated intensity (**a**) and phase (**b**) profiles of the THz beam in the plane of the EO crystal. The beam measures 330 × 316 µm.

The design of the beamline was completed using Zemax OpticStudio (2022 R2.02), allowing us to design and optimize the layout. This enabled us to confirm the expected pump beam size at the point of incidence with the pump rejection mirror, informing the required diameter of the rejection hole, as well as assessing the phase curvature in the EO detection plane. OpticStudio was also used to generate Figure 4 using the physical optics propagation (POP) simulation engine. This simulation method performs diffraction calculations to sequentially propagate the wavefront through the optical system surface by surface, taking into account the coherent nature of the propagating light, diffraction from small or fine features such as mirror edges, and wavefront phase. A Gaussian beam source with the same divergence of the experimental THz beam (∼6.36°) was defined, and POP simulations were run with 1024 × 1024 resolution; the results shown in Figure 4 are zoomed in 2× for clearer presentation.

Our beamline also utilizes four off-axis parabolic mirrors as well as an additional flat THz mirror. The first mirror is the 15° off-axis parabolic mentioned before, which allows the THz beam to diverge and fill the 50.8 mm aperture of the parabolic mirrors. This mirror collimates the THz beam and focuses the pump beam. The second mirror is a flat mirror

with a 1 mm hole drilled in the center. This hole allows for the rejection of the tightly focused pump beam with minimal clipping; a water-cooled beam dump safely disposes of the pump light. Exposing the system to 15 W of pump light resulted in pump clipping of 335 mW, or 2.2% of the total power, a considerable improvement on the 21% clipping observed previously in the conventional beamline. The clipped pump light is weak enough to be rejected using one or two sheets of paper (standard printing paper of $\simeq$0.11 mm thickness), removing the need for FZSi filters although introducing increasing losses at the higher frequencies (see, e.g., [36]). In addition, the reduced size of the rejection hole and increased THz beam size result in a reduced loss of THz radiation through the hole. We also note that, in our setup, the chopper was placed before the THz rectification process to reduce the thermal load on the generation crystal. However, in this way, the pump scattering is amplitude-modulated by the chopper, and it can, therefore, contribute to the detection noise. The rest of the setup is comparable to the conventional scheme: a second parabolic mirror placed after the flat THz mirror focuses the THz beam into a sampling spot, a third parabolic mirror recollimates the beam, and a final fourth parabolic mirror refocuses into the detection plane. This final mirror, as in the conventional setup has a hole in the center for injection of the probe beam. A knife-edge measurement of the THz beam after collimation resulted in a $1/e^2$ beam diameter of 45.22 mm. The beam fills the aperture of the mirrors almost entirely, resulting in minimal losses from the pump rejection hole whilst also avoiding clipping of the THz beam on the outer edge of the mirror.

To calculate the THz losses through the pump rejection hole, the THz beam was modelled as a Gaussian beam. Our design is expected to introduce a loss of <1%, compared to $\simeq$6% from the conventional beamline design.

5. Cooling

Multi-photon absorption limits the conversion efficiency in the optical rectification process, resulting in the generation of free carriers and heat [21,22,37]. The latter can result in thermal damage of the crystal or crystal coating and thermal lensing, while the former can directly reduce the power of the emerging THz radiation. In GaP pumped with 1030 nm, three-photon absorption dominates as two-photon absorption (2PA) is only possible via indirect bandgap absorption [37]. However, 2PA is still observed at high pump intensities [22,38]. As phonon occupation probability is temperature-dependent and indirect bandgap absorption requires assistance from the simultaneous absorption or emission of a phonon, 2PA is also strongly temperature-dependent [39]. Hence, cooling the crystal leads to a reduction in 2PA and thus improvements in THz emission.

It has been shown that cryogenically cooling GaP can indeed improve conversion efficiency and bandwidth of the generated THz radiation [22,40] and greatly reduce thermal lensing in GaP under high pump power. While this is of course a desirable improvement, it does require the use of cryogenic equipment, increasing the complexity of the system and requiring constant maintenance. For this reason, we sought to investigate whether improvements in THz generation can be gained by water-cooling GaP—akin to what is reported in [41].

Through initial measurements, we found that GaP absorbs substantial amounts of pump energy, leading to rapid heating of the crystal. We designed a water-cooled mount for the GaP crystal machined from copper. The mount features channels to allow for the ingress and egress of cooled water, enabling the copper mount to dump heat into the cooling loop. Our laser, like most high-power laser sources, requires water cooling to operate. As such, the cooling loop required to cool the GaP was already present in our experiment and is likely present in any experiments working under similar conditions. Our measurements, shown in Figure 5, show a significant increase in the THz generation efficiency when cooling the GaP crystal.

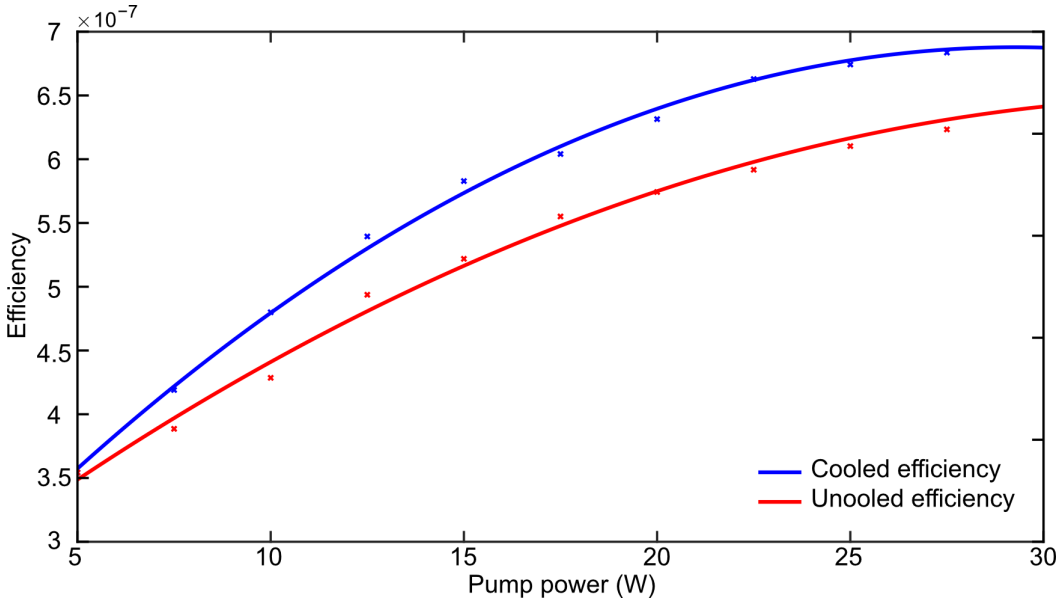

Figure 5. Efficiency of THz generation for cooled (blue) and uncooled GaP (red).

Measurements taken of the crystal surface with a thermal camera (Optris Xi 400, Optris, Berlin, Germany) show that water-cooling substantially reduces heat accumulation in the crystal. (Figure 6a,b). These images clearly show the rapid heating of the entire crystal surface without cooling and the development of a hot spot where the pump beam is incident on the surface of the crystal. The peak temperature of the crystal reaches 47.3 °C after 7 min of exposure to 25 W average power. On the other hand, after the same exposure time to the same pump power the cooled crystal shows negligible heating, maintaining an almost even temperature across the crystal over the same time period. Even at the point of pump beam incidence, we observed a temperature increase of only 1.7 °C above ambient temperature. Far field images of the beam profile after transmission through the crystal were also taken (via the Genetec Beamage 4M: Figure 6c,d). These were taken at an average pump power of 23.5 W and show considerable thermal lensing in the uncooled case. This leads to an increase in beam size as well as beam aberrations with much of the beam's intensity being split into two lobes, similar to what was also observed in [22,41], resulting in the aforementioned increased clipping of the beam during pump rejection, subsequently requiring more filtering following pump rejection. On the other hand, the beam-following transmission through the water-cooled crystal shows very little degradation with the majority of the beam intensity remaining in the central portion, allowing for effective pump rejection via geometric filtering.

THz measurements were recorded with and without crystal cooling to determine how the latter affects the signal-to-noise ratio (SNR), measured across the main peak of the THz pulse as described in [42]. At the moderate pump power of ≃13 W, where thermal lensing does not greatly affect the beam quality, the SNR is similar for the cooled and the uncooled cases. With a repetition rate of 100 kHz, SNRs of ≃270 and ≃265 were calculated for the cooled and uncooled conditions respectively, while at a 200 kHz repetition rate (with the same pump power), the SNRs were ≃109 and ≃110, respectively. On the contrary, a noticeable difference in SNRs was observed between measurements with the cooled and uncooled crystal at the higher ≃28 W pump power, where the thermal effects play a major role. For the 100 kHz repetition rate case shown in Figure 7, cooled and uncooled SNRs of ≃505 and ≃265, respectively, were recorded. For the 200 kHz case, the measured SNRs were ≃187 and ≃60. It is worth noting that the pump and the probe energies at 200 kHz are half those at 100 kHz; hence the measured THz field decreases, as expected, by a factor of $\simeq 2^{3/2}$, resulting in a decreased SNR. On the other hand, the SNR does not increase as expected with increasing power (and consequently pump and probe energies). This is likely

due to the increase in the scattering of the spatially degraded pump beam, which is picked up by the detector. Indeed, its contribution cannot be rejected by the lock-in amplifier.

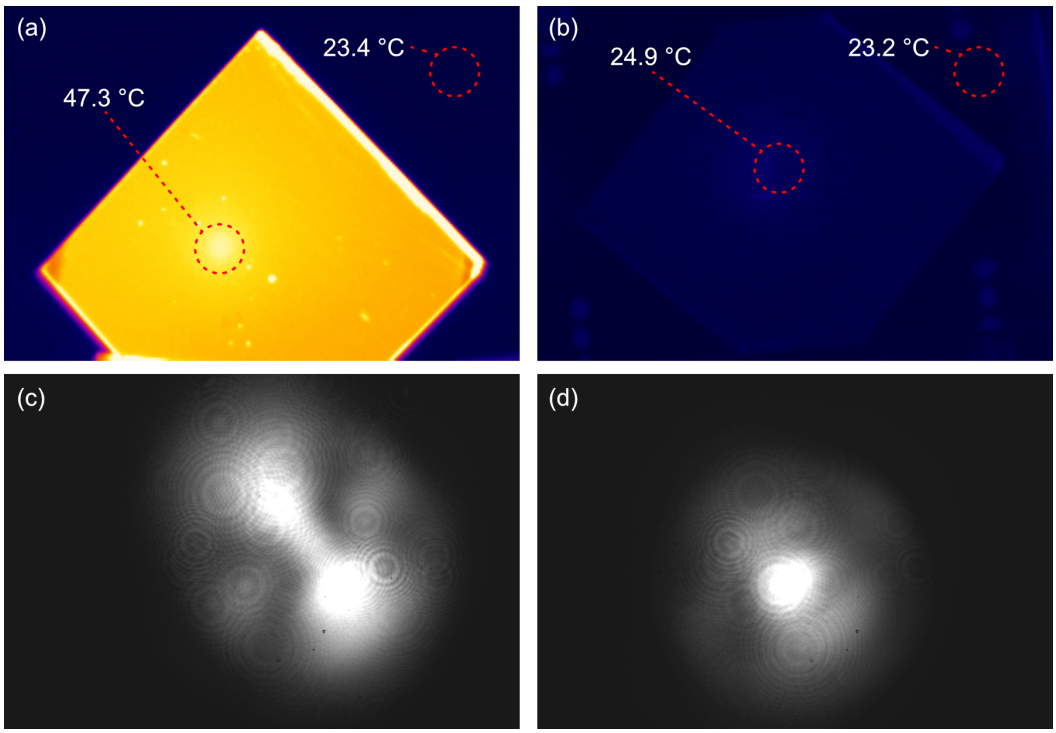

Figure 6. Comparison of cooled vs. uncooled GaP crystal. (**a**) Thermal image of crystal surface after 7 min of exposure to 25 W average pump power. (**b**) Thermal image of crystal surface in water-cooled mount after 7 min of exposure to 25 W average pump power. (**c**) Far-field image of 23.5 W pump beam after transmission through uncooled crystal. Substantial thermal lensing is evident, resulting in beam aberrations and an increase of beam size. (**d**) Far-field image of 23.5 W pump beam after transmission through water-cooled crystal. Minimal thermal lensing is observed.

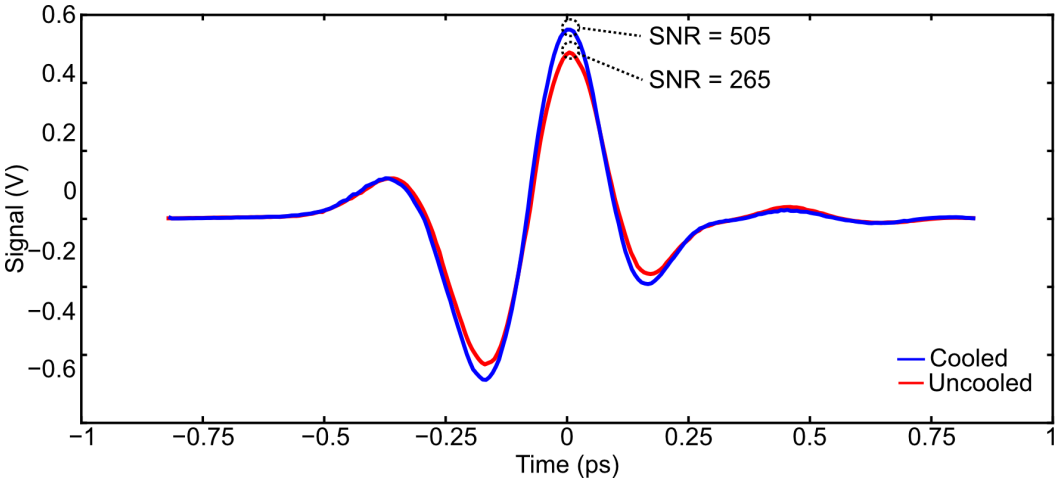

Figure 7. THz traces taken with cooled (blue) and uncooled (red) GaP at a pump power of 28 W. The scattered light resulting from thermal lensing leads to a reduction in the SNR in THz traces taken under these conditions.

6. Probe Compression

The detection bandwidth of electro-optic sampling and the temporal resolution of the resulting measurement are limited by the finite duration of the probing pulse. The finite nature of the probe pulse's duration results in a frequency response [43]

$$F(\Omega) = A_{opt}(\Omega)\chi^{(2)}(\Omega)\Delta\Phi(\Omega) \tag{1}$$

where

$$A_{opt}(\Omega) = \frac{\sqrt{\pi}}{\tau_{probe}} exp\left(-\frac{\Omega^2\tau_{probe}^2}{4}\right) \tag{2a}$$

$$\Delta\Phi = \frac{exp(-i\Delta k(\Omega)L_{det}) - 1}{i\Delta k(\Omega)} \tag{2b}$$

are the autocorrelation of the Gaussian probe pulse with duration τ_{probe} and the frequency-dependent mismatch factor, respectively. Here, Ω is the THz frequency, $\chi^{(2)}$ is the second-order susceptibility of the electro-optic crystal, L_{det} is the crystal thickness, and $\Delta k = k(\omega_{probe}) + k(\Omega) - k(\omega_{probe} - \Omega)$ is the mismatch term between the probe field, the THz field, and the frequency-difference wave vectors [43]. A_{opt} acts as a low-pass filter whose cutoff frequency depends on the probe pulse duration τ_{probe}. As such, shorter probe pulse durations result in a broader passband, thus increasing the detection bandwidth. It is therefore desirable to compress the probe pulse to achieve an optimal detection bandwidth, increasing the usable spectrum of the THz-TDS system. While this has been carried out in previous experiments using, e.g., hollow-core fibers [15] or multi-pass cell compressor [32], we decided to generate a compressed probe pulse using a two-stage compression technique allowed by the resources already available in the lab. First, an optical parametric amplifier (OPA; Orpheus-F, Light Conversion) is used to generate 2060 nm light; later, a second harmonic generation in a BBO crystal up-converts it back to 1030 nm. Our OPA generates a 2060 nm idler beam with a FWHM bandwidth of around 123 nm, which, under transform-limited conditions, results in a pulse duration of $\simeq$50 fs. Unfortunately, the OPA's idler output is not transform-limited but is instead chirped upon emission from the OPA system. To compensate for this, we introduced two Zinc Selenide (ZnSe) windows in the beam path, angling these to change the path length through the windows until optimal dispersion compensation was reached. The beam is then focused into a 0.5 mm thick BBO crystal, and the 2060 nm pump light is separated from the generated 1030 nm light using suitably coated separators (Layertec, Mellingen, Germany). We judge when optimal dispersion compensation is achieved by observing the power of the 1030 nm generated. The angle of the ZnSe windows is tuned to maximum SHG output is achieved.

Following generation, the temporally compressed 1030 nm pulse's duration is measured using the frequency-resolved optical gating technique (FROG). This measurement resulted in a pulse duration of $\simeq$56 fs, showing that we have achieved a compression ratio of $\simeq$3. The results of the FROG pulse measurement are shown in Figure 8. The FWHM bandwidth of the pulse is $\simeq$29 nm, corresponding to a transform-limited pulse duration of 53 fs. This confirms that the compressed pulse is indeed very close to the transform limit.

THz measurements taken using this compressed pulse to probe the THz show finer temporal resolution and a wider detected THz bandwidth when compared to traces taken with an uncompressed probe (Figure 9). From the increased THz bandwidth in the measurement with the compressed probe pulse it is clear that a probe duration of 245 fs is not sufficient to detect the full generated THz spectrum. Also shown are results from simulations performed by following the method described in [43], confirming the relationship found in our experiments.

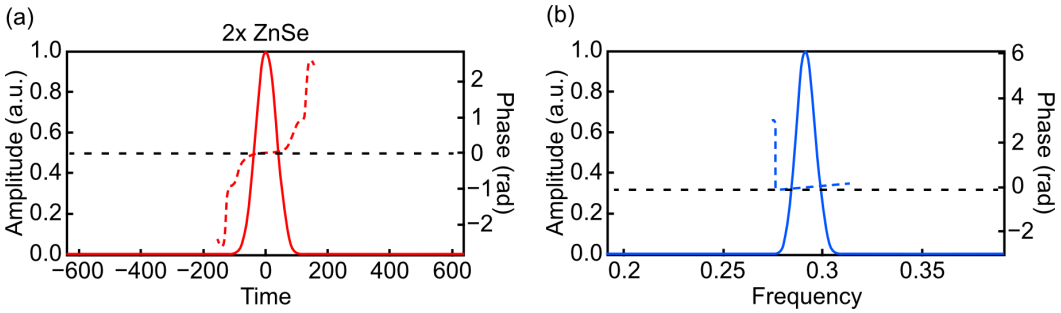

Figure 8. FROG scan of the compressed probe pulse. (**a**) shows the amplitude of the pulse in the time domain. The dashed red line indicates the phase of the pulse. (**b**) shows the frequency spectrum of the pulse. Again, the dashed blue line indicates the phase of the pulse. The dashed black lines indicate the position of the zero phase (shown on the right ordinate). The lines indicating the phase of the pulse are almost ideally flat across the pulse profile, indicating the pulse is free of chirp.

Other experimental parameters were kept identical in both measurements. Improvements in temporal resolution are desirable in spectroscopic applications as they allow for the detection of spectral features across a broader bandwidth.

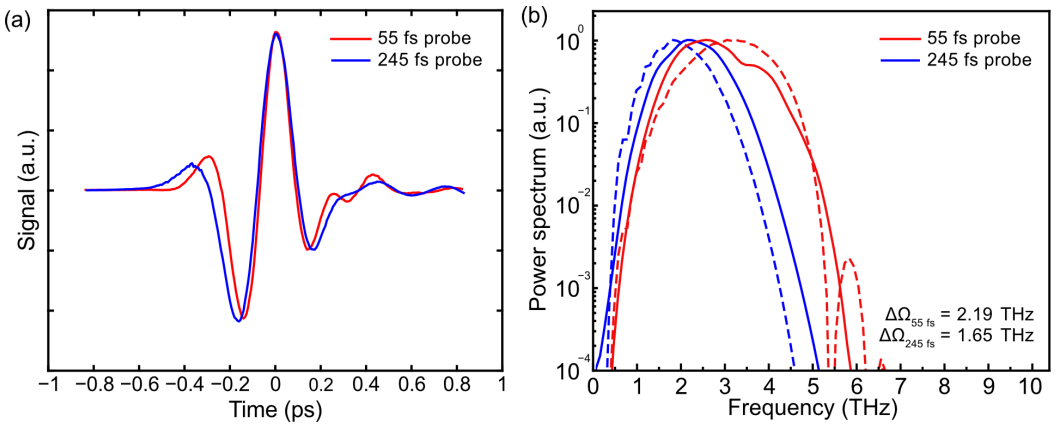

Figure 9. Comparison of THz traces taken with a 55 fs probe and a 245 fs probe. (**a**) Time-domain traces were taken with compressed (red) vs. uncompressed (blue) probe pulses. The improved resolution of the trace taken with a compressed probe is visible. The initial rise in the region between -0.1 ps and -0.4 ps shows a sharper definition in the compressed case. (**b**) Experimental (solid) and simulated (dashed) frequency spectra of the THz field probed with compressed (red) and uncompressed (blue) probe pulses. The THz trace recorded with a compressed probe exhibits $\simeq$0.54 THz greater FWHM bandwidth compared to the uncompressed case. We note that the figure has been zoomed in to highlight the difference in detection bandwidth between the compressed and uncompressed probe pulse; the noise floor is not visible in the figure and lies at ~ -60 dB.

7. Conclusions

To conclude, we have presented our THz-TDS system designed for pumping with high average power sources such as Yb-doped laser. Through the use of a redesigned THz beamline and water-cooling of the GaP generation crystal, the pump is effectively rejected and the signal-to-noise ratio improved by a factor of almost 2.

Pulse compression based on a commercial OPA allowed us to use a 55 fs, resulting in $\simeq$0.5 THz broader detected spectrum (at -3 dB). The proposed improvements are carried out using instruments commonly found in laboratories using high average power laser sources and off-the-shelf components, introducing minimal additional complexity to existing THz-TDS designs. As such, these improvements represent solutions that are feasibly applicable to many THz-TDS systems utilizing high average pump power.

Author Contributions: L.H. and M.C. designed the experiment. L.H. performed the measurements with contributions from D.A. and M.C. L.H. and M.C. analyzed the data and interpreted the results. D.A., D.F., M.P. and M.C. provided technical support to the experiment, data analysis, and interpretation of the results. L.H. and M.C. drafted the manuscript. All authors contributed to writing the final version of the manuscript. M.C. supervised the research activity. All authors have read and agreed to the published version of the manuscript.

Funding: L.H and M.C. acknowledge the support from the Defence Science and Technology Laboratory (DSTL) (scholarship number DSTLX-1000144632). M.C. acknowledges the support from UK Research and Innovation (UKRI), as the UK Engineering and Physical Sciences Research Council (EPSRC) (Fellowship "In-Tempo" EP/S001573/1) and Innovate UK, Application Number PN 10001572 (HiQuED). D.A. acknowledges the support from Innovate UK, Application Number PN 10001572 (HiQuED) and from the University of Glasgow Impact Acceleration Account (EP/X525716/1). D.F. acknowledges support from the Royal Academy of Engineering; M.P. acknowledges support from the Leverhulme Trust, Research Project Grant number RPG-2022-090 and from the DEVCOM ARL Army Research Office, Grant number W911NF2310313.

Institutional Review Board Statement: Not applicable.

Informed Consent Statement: Not applicable.

Data Availability Statement: The original data presented in the study are openly available at https://doi.org/10.5525/gla.researchdata.1675.

Conflicts of Interest: The authors declare no conflicts of interest.

References

1. Zhang, X.C.; Xu, J. *Introduction to THz Wave Photonics*, 1st ed.; Springer: New York, NY, USA, 2015.
2. Neu, J.; Schmuttenmaer, C.A. Tutorial: An Introduction to Terahertz Time Domain Spectroscopy (THz-TDS). *J. Appl. Phys.* **2018**, *124*, 231101. [CrossRef]
3. Mittleman, D.M. Perspective: Terahertz Science and Technology. *J. Appl. Phys.* **2017**, *122*, 230901. [CrossRef]
4. Cherkasova, O.; Konnikova, M.; Kistenev, Y.; Vaks, V.; Coutaz, J.L.; Shkurinov, A. Terahertz Spectroscopy of Biological Molecules in Solid, Liquid, and Gaseous States. In *Molecular and Laser Spectroscopy*; Gupta, V., Ed.; Elsevier: Amsterdam, The Netherlands, 2022; Volume 3, pp. 433–478.
5. Davies, A.G.; Burnett, A.D.; Fan, W.; Linfield, E.H.; Cunningham, J.E. Terahertz Spectroscopy of Explosives and Drugs. *Mater. Today* **2008**, *11*, 18–26. [CrossRef]
6. Peiponen, K.E.; Zeitler, A.; Kuwata-Gonokami, M. (Eds.) *Terahertz Spectroscopy and Imaging*; Springer: Berlin/Heidelberg, Germany, 2013; Volume 171.
7. Jepsen, P.; Cooke, D.; Koch, M. Terahertz Spectroscopy and Imaging—Modern Techniques and Applications. *Laser Photonics Rev.* **2011**, *5*, 124–166. [CrossRef]
8. Gowen, A.; O'Sullivan, C.; O'Donnell, C. Terahertz Time Domain Spectroscopy and Imaging: Emerging Techniques for Food Process Monitoring and Quality Control. *Trends Food Sci. Technol.* **2012**, *25*, 40–46. [CrossRef]
9. Pereira, M.F.; Anfertev, V.; Shevchenko, Y.; Vaks, V. Giant controllable gigahertz to terahertz nonlinearities in superlattices. *Sci. Rep.* **2020**, *10*, 15950. [CrossRef] [PubMed]
10. Vaks, V.; Anfertev, V.; Chernyaeva, M.; Domracheva, E.; Yablokov, A.; Maslennikova, A.; Zhelesnyak, A.; Baranov, A.; Schevchenko, Y.; Pereira, M.F. Sensing nitriles with THz spectroscopy of urine vapours from cancers patients subject to chemotherapy. *Sci. Rep.* **2022**, *12*, 18117. [CrossRef] [PubMed]
11. Liu, H.B.; Zhong, H.; Karpowicz, N.; Chen, Y.; Zhang, X.C. Terahertz Spectroscopy and Imaging for Defense and Security Applications. *Proc. IEEE* **2007**, *95*, 1514–1527. [CrossRef]
12. Beck, M.; Schäfer, H.; Klatt, G.; Demsar, J.; Winnerl, S.; Helm, M.; Dekorsy, T. Impulsive Terahertz Radiation with High Electric Fields from an Amplifier-Driven Large-Area Photoconductive Antenna. *Opt. Express* **2010**, *18*, 9251–9257. [CrossRef]
13. Lu, P.K.; Turan, D.; Jarrahi, M. High-Power Terahertz Pulse Generation from Bias-Free Nanoantennas on Graded Composition InGaAs Structures. *Opt. Express* **2022**, *30*, 1584–1598. [CrossRef]
14. Oh, T.I.; Yoo, Y.J.; You, Y.S.; Kim, K.Y. Generation of Strong Terahertz Fields Exceeding 8 MV/Cm at 1 kHz and Real-Time Beam Profiling. *Appl. Phys. Lett.* **2014**, *105*, 041103. [CrossRef]
15. Piccoli, R.; Rovere, A.; Jeong, Y.G.; Jia, Y.; Zanotto, L.; Légaré, F.; Schmidt, B.E.; Morandotti, R.; Razzari, L. Extremely Broadband Terahertz Generation via Pulse Compression of an Ytterbium Laser Amplifier. *Opt. Express* **2019**, *27*, 32659–32665. [CrossRef] [PubMed]
16. Koulouklidis, A.D.; Lanara, C.; Daskalaki, C.; Fedorov, V.Y.; Tzortzakis, S. Impact of Gas Dynamics on Laser Filamentation THz Sources at High Repetition Rates. *Opt. Lett.* **2020**, *45*, 6835–6838. [CrossRef] [PubMed]

17. Hebling, J.; Stepanov, A.; Almási, G.; Bartal, B.; Kuhl, J. Tunable THz Pulse Generation by Optical Rectification of Ultrashort Laser Pulses with Tilted Pulse Fronts. *Appl. Phys. B* **2004**, *78*, 593–599. [CrossRef]
18. Huang, S.W.; Granados, E.; Huang, W.R.; Hong, K.H.; Zapata, L.E.; Kärtner, F.X. High Conversion Efficiency, High Energy Terahertz Pulses by Optical Rectification in Cryogenically Cooled Lithium Niobate. *Opt. Lett.* **2013**, *38*, 796–798. [CrossRef] [PubMed]
19. O Krizsán, G.; Tibai, Z.; Hebling, J.; Pálfalvi, L.; Almási, G.; Tóth, G. Lithium Niobate and Lithium Tantalate Based Scalable Terahertz Pulse Sources in Reflection Geometry. *Opt. Express* **2020**, *28*, 34320–34327. [CrossRef] [PubMed]
20. Wu, Q.; Zhang, X.C. 7 Terahertz Broadband GaP Electro-Optic Sensor. *Appl. Phys. Lett.* **1997**, *70*, 1784–1786. [CrossRef]
21. Hoffmann, M.C.; Yeh, K.L.; Hebling, J.; Nelson, K.A. Efficient Terahertz Generation by Optical Rectification at 1035 Nm. *Opt. Express* **2007**, *15*, 11706–11713. [CrossRef] [PubMed]
22. Hekmat, N.; Vogel, T.; Wang, Y.; Mansourzadeh, S.; Aslani, F.; Omar, A.; Hoffmann, M.; Meyer, F.; Saraceno, C.J. Cryogenically Cooled GaP for Optical Rectification at High Excitation Average Powers. *Opt. Mater. Express* **2020**, *10*, 2768–2782. [CrossRef]
23. Negel, J.P.; Hegenbarth, R.; Steinmann, A.; Metzger, B.; Hoos, F.; Giessen, H. Compact and Cost-Effective Scheme for THz Generation via Optical Rectification in GaP and GaAs Using Novel Fs Laser Oscillators. *Appl. Phys. B* **2011**, *103*, 45–50. [CrossRef]
24. McNee, I.; Tekavec, P.; Kozlov, V.; Markelz, A.; George, D.; Schunemann, P.G. Tunable Narrowband THz Generation in Orientation Patterned Gallium Phosphide for THz Anisotropy Identification. In Proceedings of the Nonlinear Frequency Generation and Conversion: Materials and Devices XVIII Conference, San Francisco, CA, USA, 2–7 February 2019; Volume 10902. [CrossRef]
25. Dai, J.; Zhang, J.; Zhang, W.; Grischkowsky, D. Terahertz Time-Domain Spectroscopy Characterization of the Far-Infrared Absorption and Index of Refraction of High-Resistivity, Float-Zone Silicon. *J. Opt. Soc. Am. B* **2004**, *21*, 1379–1386. [CrossRef]
26. Bludau, W.; Onton, A.; Heinke, W. Temperature Dependence of the Band Gap of Silicon. *J. Appl. Phys.* **1974**, *45*, 1846–1848. [CrossRef]
27. Sulzer, P.; Oguchi, K.; Huster, J.; Kizmann, M.; Guedes, T.L.M.; Liehl, A.; Beckh, C.; Moskalenko, A.S.; Burkard, G.; Seletskiy, D.V.; et al. Determination of the Electric Field and Its Hilbert Transform in Femtosecond Electro-Optic Sampling. *Phys. Rev. A* **2020**, *101*, 033821. [CrossRef]
28. Mansell, J.D.; Hennawi, J.; Gustafson, E.K.; Fejer, M.M.; Byer, R.L.; Clubley, D.; Yoshida, S.; Reitze, D.H. Evaluating the Effect of Transmissive Optic Thermal Lensing on Laser Beam Quality with a Shack–Hartmann Wave-Front Sensor. *Appl. Opt.* **2001**, *40*, 366–374. [CrossRef]
29. Petersen, E.B.; Shi, W.; Chavez-Pirson, A.; Peyghambarian, N.; Cooney, A.T. Efficient Parametric Terahertz Generation in Quasi-Phase-Matched GaP through Cavity Enhanced Difference-Frequency Generation. *Appl. Phys. Lett.* **2011**, *98*, 121119. [CrossRef]
30. Chang, G.; Divin, C.J.; Liu, C.H.; Williamson, S.L.; Galvanauskas, A.; Norris, T.B. Power Scalable Compact THz System Based on an Ultrafast Yb-doped Fiber Amplifier. *Opt. Express* **2006**, *14*, 7909–7913. [CrossRef]
31. Li, J.; Chai, L.; Shi, J.; Liu, F.; Liu, B.; Xu, B.; Hu, M.; Li, Y.; Xing, Q.; Wang, C.; et al. Generation of 0.3 mW High-Power Broadband Terahertz Pulses from GaP Crystal Pumped by Negatively Chirped Femtosecond Laser Pulses. *Laser Phys. Lett.* **2013**, *10*, 125404. [CrossRef]
32. Meyer, F.; Hekmat, N.; Vogel, T.; Omar, A.; Mansourzadeh, S.; Fobbe, F.; Hoffmann, M.; Wang, Y.; Saraceno, C.J. Milliwatt-Class Broadband THz Source Driven by a 112 W, Sub-100 Fs Thin-Disk Laser. *Opt. Express* **2019**, *27*, 30340–30349. [CrossRef] [PubMed]
33. Xu, J.; Globisch, B.; Hofer, C.; Lilienfein, N.; Butler, T.; Karpowicz, N.; Pupeza, I. Three-Octave Terahertz Pulses from Optical Rectification of 20 Fs, 1 µM, 78 MHz Pulses GaP. *J. Phys. B At. Mol. Opt. Phys.* **2018**, *51*, 154002. [CrossRef]
34. Ding, Y. Quasi-Single-Cycle Terahertz Pulses Based on Broadband-Phase-Matched Difference-Frequency Generation in Second-Order Nonlinear Medium: High Output Powers and Conversion Efficiencies. *IEEE J. Sel. Top. Quantum Electron.* **2004**, *10*, 1171–1179. [CrossRef]
35. Meyer, F.; Hekmat, N.; Mansourzadeh, S.; Fobbe, F.; Aslani, F.; Hoffmann, M.; Saraceno, C.J. Optical Rectification of a 100 W Average Power Mode-Locked Thin-Disk Oscillator. *Opt. Lett.* **2018**, *43*, 5909–5912. [CrossRef]
36. Peccianti, M.; Fastampa, R.; Mosca Conte, A.; Pulci, O.; Violante, C.; Łojewska, J.; Clerici, M.; Morandotti, R.; Missori, M. Terahertz Absorption by Cellulose: Application to Ancient Paper Artifacts. *Phys. Rev. Appl.* **2017**, *7*, 064019. [CrossRef]
37. Liu, F.; Li, Y.; Xing, Q.; Chai, L.; Hu, M.; Wang, C.; Deng, Y.; Sun, Q.; Wang, C. Three-Photon Absorption and Kerr Nonlinearity in Undoped Bulk GaP Excited by a Femtosecond Laser at 1040 Nm. *J. Opt.* **2010**, *12*, 095201. [CrossRef]
38. Pyshkin, S.L.; Ferdman, N.A.; Radautsan, S.I.; Kovarsky, V.A.; Vitiu, E.V. Many-Quantum Absorption in Gallium Phosphide. *Opto-electronics* **1970**, *2*, 245–249. [CrossRef]
39. Nathan, V.; Mitra, S.S.; Guenther, A.H. Review of Multiphoton Absorption in Crystalline Solids. *J. Opt. Soc. Am. B* **1985**, *2*, 294–316. [CrossRef]
40. Huang, J.; Li, Y.; Gao, Y.; Li, G.; Huang, Z.; Chu, J.; Andreev, Y. High Efficient Terahertz Generation from Cryogenic Gallium Phosphide Based on Collinear Difference Frequency. In Proceedings of the Fifth International Symposium on Laser Interaction with Matter Conference, Changsha, China, 11–14 November 2018; Volume 11046, p. 76. [CrossRef]
41. Wulf, M.S.F.; Meyer, G.; Saraceno, C.J.; Kärtner, F.X. Novel High Power THz Sources Driven by Mode-Locked Thin-Disk Lasers. Doctoral Thesis, Ruhr-Universitat Bochum, Bochum, Germany, 2020.

42. Naftaly, M.; Dudley, R. Methodologies for Determining the Dynamic Ranges and Signal-to-Noise Ratios of Terahertz Time-Domain Spectrometers. *Opt. Lett.* **2009**, *34*, 1213–1215. [CrossRef]
43. Tomasino, A.; Parisi, A.; Stivala, S.; Livreri, P.; Cino, A.C.; Busacca, A.C.; Peccianti, M.; Morandotti, R. Wideband THz Time Domain Spectroscopy Based on Optical Rectification and Electro-Optic Sampling. *Sci. Rep.* **2013**, *3*, 3116. [CrossRef]